



LETTER

Liquid foam under simple shear: Local flows in the films


To cite this article: R. Poryles *et al* 2023 *EPL* **141** 23001

View the [article online](#) for updates and enhancements.

You may also like

- [A phase-field study of the effect of local deformation velocity on lithiation-induced stress in wire-like structures](#)
Kai Zhang, Yong Li, Feng Wang et al.
- [Compressive properties of biomedical open-cell Zn foam](#)
Dingding Wang, Xuan Zhang, Guyin Zu et al.
- [Preparation of bisphenol A polyarylether nitrile microporous foam](#)
Qing Qi, Yajie Lei and Xiaobo Liu

Liquid foam under simple shear: Local flows in the films

R. PORYLES^{1,2}, A. BUSSONNIÈRE^{1,3}, E. SCHAUB¹ and I. CANTAT^{1(a)} 

¹ *Univ Rennes, CNRS, IPR (Institut de Physique de Rennes), UMR 6251 - F-35000 Rennes, France*

² *ONIRIS, UMR 6144 GEPEA CNRS - F-44322 Nantes, France*

³ *Laboratoire Matière et Systèmes Complexes, Université Paris Cité, CNRS UMR 7057 - F-75013 Paris, France*

received 6 July 2022; accepted in final form 14 December 2022

published online 11 January 2023

Abstract – Predicting the effective viscosity of a foam as a function of its bubble size, liquid fraction and chemical composition is still an open question. The confinement of the liquid phase between the bubbles is expected to strongly enhance the local deformation rates. However, these local deformations are induced by interfacial stresses, which are limited by the surface tension accessible range: above a critical bubble size and/or shear rate, it is impossible to shear the whole film separating the bubbles. In this paper, we investigate this large bubble regime by imposing a simple shear to a minimal foam made of five interconnected films. We present a new local deformation pattern, with a relaxation process lasting long after the motor stops, that we characterize for a large range of shear rate and for different foaming solutions. A direct evidence of the absence of shear during the relaxation has been obtained for one solution. At 10 s^{-1} , this original large bubble regime should be relevant for foams with bubbles larger than 300 microns.

Copyright © 2023 EPLA

Introduction. – The liquid foam belongs to the class of the soft visco-elasto-plastic materials [1]. Under an imposed shear, the stress depends on the shear rate and can be well fitted by a Herschel-Bulkley law [2,3], with a constant yield stress σ_y at low shear rate. However, neither the exponent nor the prefactor of this phenomenological law can be predicted with certainty yet, despite recent efforts of the scientific community working on foams, emulsions and more generally on complex fluids [4–7]. The high effective viscosity of foams, which can be defined in steady shear experiment as $(\sigma - \sigma_y)/(d\varepsilon/dt)$ with σ the stress and ε the deformation, is directly related to the confinement of the continuous phase. Schematically, if the bubbles slide over each other with negligible in-plane deformation of their interface, as assumed in [4], the local shear rate in the continuous phase scales as the global imposed shear rate multiplied by the ratio between the bubble size L and the thickness of the film h . This ratio is usually of the order of 1000, leading to a drastic increase of local shear rate in thin films.

This localization of the shear in the thin liquid films separating the bubbles is associated with a velocity difference $\delta v \sim \dot{\varepsilon}L$ between both interfaces of the sheared film, and to a viscous stress $\eta \delta v/h \sim \eta \dot{\varepsilon}L/h$, with η the bulk viscosity. The tangential force (per unit length)

acting on the interface of a sheared film of length L scales thus as $\eta \dot{\varepsilon}L^2/h$ and must be balanced by the surface tension difference $\delta\gamma$ between both ends of the film. However, this surface tension difference cannot be higher than $\delta\gamma^{max} = \gamma_w$, with $\gamma_w = 72\text{ mN/m}$ the surface tension of the pure water/air interface. The simple sliding motion of a bubble over its neighboring bubble, as a soft solid would have, is thus not possible at large bubble size, or large imposed shear rate, and another velocity field must be observed in this regime.

Recent measurements and models on soap films held on solid frames allowed important progress [4,8–12]. However, the value of the local shear when a global shear is imposed to a foam, and its localization in the continuous phase, are still open questions. A prediction of a shear localization in the vicinity of the menisci has been recently proposed in [12] in the large bubble limit, but no direct measurements were performed. Moreover, the imposed deformations in this previous study did not properly mimic a simple shear. Indeed, under a shear deformation ε below the yield strain, the total interface area in a foam increases as ε^2 , which is at the origin of the foam elasticity. Each individual film area varies in contrast as ε [13,14]. For a small deformation, the fluctuations of the total interface area of each bubble is thus negligible in comparison with the individual film area fluctuation, and the total area of each interface can be considered as constant when addressing the question of film dynamics. This total area

^(a)E-mail: isabelle.cantat@univ-rennes1.fr (corresponding author)

conservation was clearly violated in [12], which potentially leads to different film dynamics.

In this study, we use a home-made setup respecting this area constraint to unravel the local flow associated to an imposed shear deformation, in a five films assembly. In order to be in the large bubble regime, we impose $h \sim 10^{-6}$ m, $\eta = 1.5 \cdot 10^{-3}$ Pa \cdot s, $L = 6 \cdot 10^{-3}$ m and $\dot{\epsilon} \sim 10$ s $^{-1}$, so that $\eta \dot{\epsilon} L^2/h \sim 0.5$ N/m $\gg \gamma_w$. We show that the global shear turns locally into film compression and stretching deformations, which relax via surfactant transfers from one film to its neighbor. Surprisingly, these surfactant transfers lead to an interface compression in the film that evolves at constant total area. This original deformation pattern should be relevant for a foam in the large bubble regime. Assuming a 100 nm film thickness and a maximal tension difference of 10 mN/m, this regime should be reached for a bubble diameter of 300 μ m at $\dot{\epsilon} = 10$ s $^{-1}$.

Experimental set-up. – The set-up shown in fig. 1 has been used to deform an assembly of 5 soap films connected to each others along suspended menisci. The central film (index c) is horizontal and connected to the four lateral films (indices tl , tr , bl and br). The notations l/r , t/b and c indicate respectively left/right, top/bottom and central. The air/liquid interfaces on both sides of each film are also connected to each other, and constitute four continuous pieces of interface: the bottom, top, left and right interfaces (see the colored lines in fig. 1(b)). This setup has already been used in previous studies and is described in [12]. In the present study, the main imposed deformation is a shear deformation (denoted (S) in the following) preserving the total area of each of the four interfaces: the lengths of the top right and bottom left films increase as $L^{tr/bl} = L_0 + V^m(t - t^m/2)$ in the time range $[0 - t^m]$, and the lengths of the top left and bottom right films decrease as $L^{tl/br} = L_0 - V^m(t - t^m/2)$, with V^m the motor velocity and L_0 the average length of the lateral films.

We used five different foaming solutions: four with sodium dodecyl sulfate (SDS BioXtra $\leq 99\%$, Sigma-Aldrich, critical micellar concentration $cmc = 2.33$ g/L) at concentration $c_s = 2.4$ cmc and 1-dodecanol (DOH, $\leq 98\%$, Sigma-Aldrich), at concentration $c_d = [0, 15, 35, 50]$ mg/L (S_1, S_2, S_3, S_4), and one with SDS at $c_s = 1.2$ cmc, without dodecanol (S_5). Fluorescein at the concentration 0.8 g/L and glycerol (15% in volume) are added in each solution. The surface tensions and relative film elasticities measured in [15] for these solutions S_i are $\gamma_i = [38, 37, 34, 33, 38]$ mN/m and $E_i^f/(2\gamma_i) = [0.024, 0.054, 0.098, 0.143, 0.04]$.

The deformable frame is plunged into the foaming solution and removed. The motor motion begins at the time $t = 0$ taken as a reference, 16 seconds after the films formation. At this time, the films are still out of equilibrium and slowly drain because of the gravity and the capillary suction. This drainage occurs on a time scale larger than the flows induced by the imposed shear.

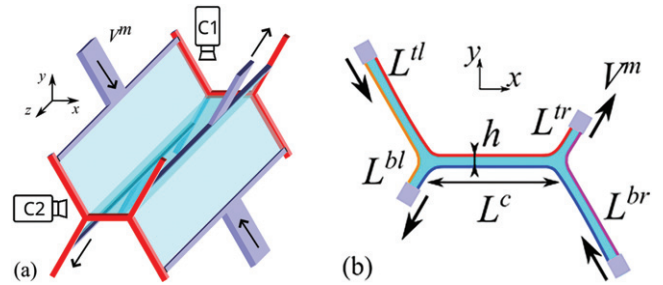


Fig. 1: (a) Scheme of the setup. Five soap films (in blue) are supported on a metallic frame (in red and purple). Their length in the z -direction is 60 mm, and the horizontal film length is 6 mm in the x -direction. The purple parts slide on the red parts, at a velocity V^m controlled by 4 motors. The camera C1 records the central film in fluorescence and the camera C2 measures the vertical position of the menisci. (b) Scheme of the films assembly in the (x, y) -plane, before the deformation. The notations l/r , t/b and c indicate respectively left/right, top/bottom and central. The black arrows show how a global shear deformation is imposed on the film assembly. The four colored lines represent the four interfaces, whose area is preserved during the deformation.

The fluorescence of the central film is excited with a blue light and the emission intensity is observed from the top using a camera (MV1-D1312-160-CL12, PhotonFocus, 950×544 , C1 in fig. 1(a)), at 280 frames per second, using a filter centered at the fluorescein emission wavelength. The image brightness is due to the fluorescence emitted by the entire thickness of the film, so the gray level indicates the film thickness. A laser at 488 nm is focused on the film to photobleach the fluorescein across the whole film at the desired place, thus producing dark spots of diameter 50 μ m in the image of the central film. These small dark volumes follow the velocity field of the liquid phase: the velocity of the spot center is the velocity of the film, averaged over its thickness. The diffusion has a characteristic length scale $\sqrt{Dt} \sim 10$ μ m with $D \sim 10^{-9}$ m 2 s $^{-1}$ the diffusion coefficient and $t \sim 50$ ms the observation time scale and leads to an axisymmetric evolution of the spot intensity profile. Importantly, the observation of a non-axisymmetric evolution of the emission intensity of the pattern would be the signature of a velocity gradient across the film (see fig. 2).

The free menisci can move due to surface tension differences as observed in [12]. Their motions are therefore monitored in the xz plane with the top camera (C1) while their motion in the yz plane are followed with another camera (C2, ac A1920-155uc, Basler ace, 400×1920).

Qualitative behavior of the central film. – The imposed deformation induces a tension increase in the two stretched films, and a tension decrease in the two compressed ones. Consequently, the left meniscus moves down and the right meniscus moves up. However, these displacements are small and the shape of the film assembly remains very close to its equilibrium shape, governed by the well-known Plateau laws of minimal surfaces [13]: the

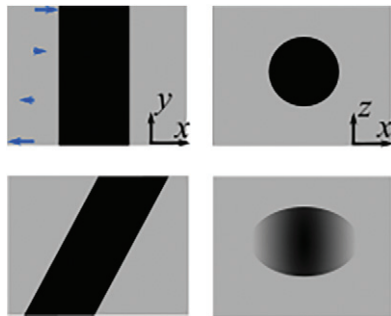


Fig. 2: Effect that a local shear deformation would have on the image of a photobleached spot. The first line shows schematic views of the spot shape just after its formation, and the second line the same views after convection during a time t by the simple shear velocity field represented by the blue arrows, in the top left figure. The left column shows a cut along a diameter in the (x, y) -plane and the right column a projection in the (x, z) -plane, mimicking what would be observed on the experimental image.

five films remain plane, move in their own plane, and intersect at an angle close to 120° . The tangential motion of the interfaces evidenced with our set-up are much more complex, as discussed below.

Images of the central film at different times are shown in fig. 3, for $V^m = 0.1$ m/s and $V^m t^m = 12$ mm, corresponding to the motor amplitude A^m . For this value of the imposed shear, a thick film strip appears on each side of the central film, extracted from the two menisci. These extracted films, denoted Frankel film in the following, are those usually observed in stretched films [11,12,16] and surprisingly appear here, even though the central film is not stretched. They remain identical and invariant in the z -direction during typically 300 ms (figs. 3(b) and (c)). Then two independent destabilization processes occur.

Hemi-circular spots of very thin film, evidenced by dark domains, appear between the meniscus and the extracted film, first at the left meniscus (fig. 3(d)), then at the right one, typically 100 ms later (fig. 3(e)). This instability has been described in [16] under the name of marginal regeneration. Its onset indicates the end of the film extraction and the beginning of its re-absorption by the meniscus [16–18]. The observed delay between the destabilization of both sides is the signature of a left/right symmetry breaking. This symmetry is broken by the gravity field for at least two reasons, whose respective role in the instability onset is not elucidated yet: i) the central film is slightly tilted, with its right boundary a fraction of mm above its left boundary; ii) the initial thicknesses of the top and bottom films are different, so the left and right compressed films moving toward the menisci are not strictly equivalent.

Another instability is observed at the boundary between the thick extracted film and the thin part of the central film, on the right side (see fig. 3(d), (e)). This instability is a Rayleigh-Taylor instability driven by the gravity, and arises when a thick domain is located above a thin one in

a soap film [19]. It is thus directly related to the small tilt of the central film.

Absence of shear in the central film during the film extraction. – The thickness of the extracted films is of the order of 3 microns. Photobleached spots produced there are highly contrasted and we analyzed the shape of such spots for the foaming solution S_4 . This solution has the highest surface elasticity and thus is the mostly likely one to exhibit a shear. In fig. 4, we show an intensity profile measured along a spot diameter as a function of time.

The intensity profile has been fitted by a Gaussian profile $I^{fit} = I_0(1 - a \exp[-(r_{x,z} - r_0)^2/w_{x,z}^2])$, for the directions x and z , respectively. In this example, the spot moves three times its diameter toward the center of the film because of the extraction of the thick film from the meniscus. The motion occurs without measurable deformation of the spot shape, which keeps the same diameters $w_x = 47 \pm 10 \mu\text{m}$ and $w_z = 50 \pm 10 \mu\text{m}$ in the x and z directions. This allows us to determine an upper bound δv^{UB} for the velocity difference δv between the top and bottom interfaces. Indeed, as shown in fig. 2, the x -diameter of the spot image increases as $\delta v t$, with t the age of the spot. The x -diameter stays at $50 \mu\text{m}$ during $t = 54$ ms with a precision given by the pixel size $\delta = 10 \mu\text{m}$, of the order of the diffusion length previously discussed. Using $\delta v^{UB} t = \delta$, we get $\delta v^{UB} = 0.4$ mm/s. This value must be compared to the expected velocity difference in the inextensible interface limit, in which the 4 interfaces are pushed by the different motors without area variation (see fig. 1(b)). In that case, the imposed shear is entirely transmitted to the liquid phase and is enhanced by the confinement. In this limit, the velocity difference between the top and bottom interfaces in the central film is twice the motor velocity, *i.e.*, $\delta v^{inex} = 200$ mm/s, three orders of magnitude larger than δv^{UB} .

The contrast is not high enough in the central part of the film for the spot shape to be analyzed. However, as the shear is imposed from the lateral films, the central part of the central film cannot be sheared if its boundaries are not. We can therefore conclude that the imposed shear is not significantly transmitted to the central film during the film extraction.

Shear transmission in the central film before the beginning of the extraction is difficult to test. It is less likely to happen at small times than during the film extraction, because the driving force, which is a tension difference between the adjacent films, is smaller, and the resisting force, proportional to $1/h$, is larger. Note also that the solution (S_4) has a larger elastic modulus than the other ones. The interfaces deformations thus lead to higher surface tension variations, and shear transmission to the bulk should thus be even smaller for the other solutions, for which the photobleaching process has not been performed. Finally, we cannot exclude a localized shear close to the meniscus, at a distance smaller 0.2 mm, as conjectured in [12]. Indeed,

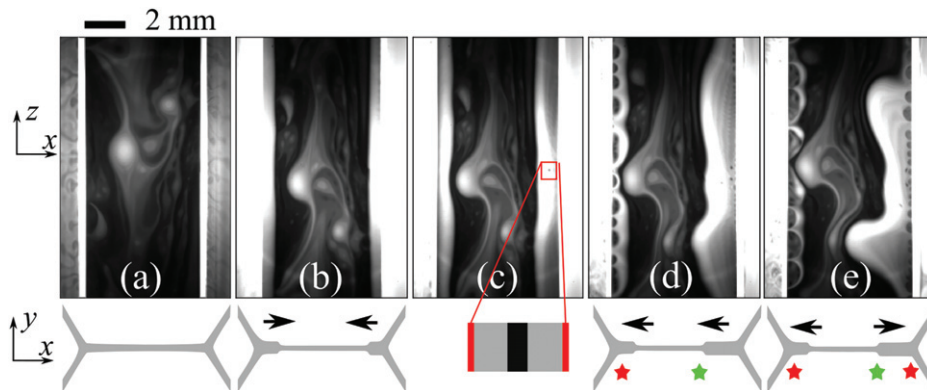


Fig. 3: Fluorescence images of the central film: (a) $t = 0$, beginning of the motor motion, (b) $t = 140$ ms, motor stops, (c)–(e) after motor stops, $t = 210$ ms, 390 ms and 640 ms. The scheme of the side view, in the (x, y) -plane is represented below with the same scale in the x -direction. The two suspended menisci appear as saturated vertical white bands in (a), 6 mm apart. The lateral films, visible in (a), are almost saturated in (b)–(e). The extracted films are the two bright bands on the left and right sides of the central film, the black arrows indicating their direction of motion. They destabilize respectively in (d) and (e), because of the marginal regeneration (red stars) and because of a Rayleigh-Taylor instability (green stars). In (c) a photobleached spot is visible in the red square, with its side view plane below. These images have been obtained using the solution S_4 and the deformation (S) with $V^m = 100$ mm/s, and $A^m = V^m t^m = 12$ mm.

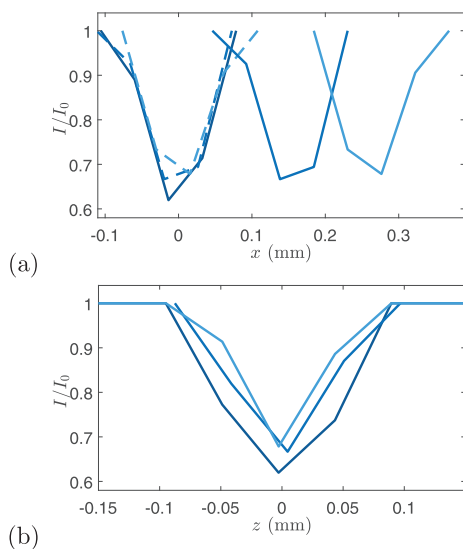


Fig. 4: Motion and deformation of a photobleached spot in the central film, for the same experiment as in fig. 3. The spot is produced at the distance 0.2 mm from the left meniscus at the time $t = 171$ ms. Intensity profiles at time [171, 207, 225] ms (from dark to light blue) (a) in the x -direction (oriented toward the film) and (b) in the z -direction. The meniscus motion is negligible in this time range. The dashed line are the same x -profiles, translated.

we have not been able to produce a spot at a distance smaller than 0.2 mm from the meniscus.

Film extraction in the central film. – As the central film is not sheared during the film extraction for the solution (S_4), both interfaces deform together and, by symmetry, the velocity is zero at the middle of the central film for the two interfaces. The left and right sides of the experiment are thus entirely decoupled. Consequently, the

deformation (U) (as upwards), in which the deformation of the top left and bottom left films are switched (the 4 motors move upwards, the two bottom films are compressed and the two top films are stretched) should lead to the same flow in the central film. This new deformation allows us to avoid gravitational destabilization of the extracted films, discussed previously, since the central film remains horizontal during the dynamic. The (U) deformation, instead of (S) is therefore used in the following to quantify the film extraction in the central film. We checked that the same result is obtained for the symmetrical deformation (D), for which the 4 motors move downwards.

As the phenomenology is the same for the other solutions, their film extraction is studied with the same protocol.

The width of the Frankel films in the central film are plotted as a function of time in fig. 5(a). The extraction begins with some delay with respect to the motor motion and it saturates at a plateau after typically 0.1 ms. Dark spots appear at the boundary between the film and the meniscus at a similar time, and indicate consistently the end of the film extraction. The maximal width reached by the Frankel films depends on the foaming solution and increases with the film elastic modulus E^f . When the extracted width is rescaled by $E^f/(2\gamma)$ all the data (excepted S_2) are superimposed within the error bar (see in fig. 5(b)). The Frankel film extraction requires a surface tension larger in the central film, at tension γ , than in the menisci, at tension $\gamma - \delta\gamma$. For a given film deformation, the tension variations are proportional to the Gibbs elasticity, which justifies qualitatively the proposed rescaling.

Note that the surface tensions of the different solutions are close to each other, so the rescaling by E^f would be of similar quality.

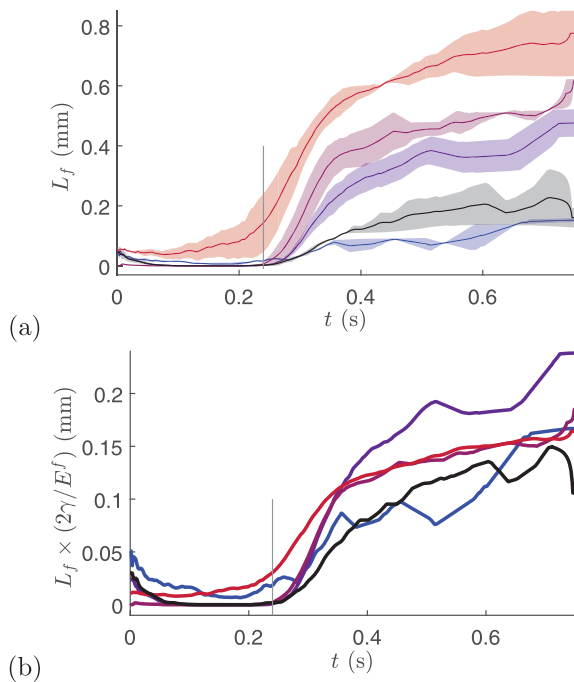


Fig. 5: Frankel film extraction during and after the imposed deformation ($V^m = 50$ mm/s, $t^m = 0.24$ s, (U) deformation) for the foaming solutions S_1 to S_4 (blue to red) and S_5 (black). The time t^m is marked by a vertical grey line on both plots. (a) Width of the Frankel film, averaged over the left and right sides (the error bars are given by the difference between both sides). (b) Same data, rescaled by the relative film elasticity $E^f/(2\gamma)$.

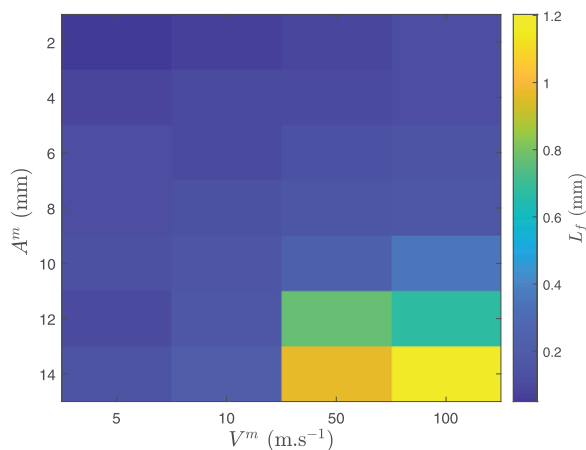


Fig. 6: Maximal extracted film width (average on both film sides) as a function of the motor amplitude $A^m = V^m t^m$ and velocity V^m , for solution S_3 and deformation (U).

The maximal Frankel film size also depends on the imposed deformation. As shown in fig. 6, it increases with the imposed motor velocity and with the motion amplitude. Note that no Frankel films are observed for small and slow deformations. A scheme of the velocity field is proposed in fig. 7 for the right part of the system.

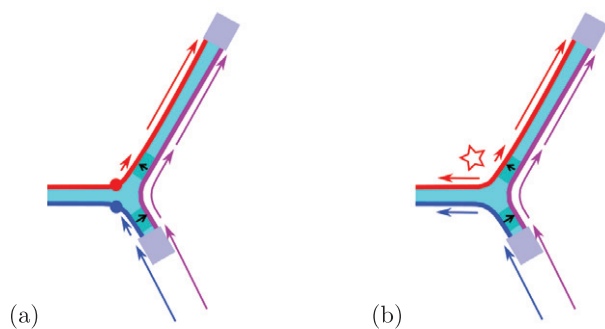


Fig. 7: Schematical representation of the interface displacement during the (U) deformation, in the right part of the system (the left part is obtained by a mirror symmetry). Each colored arrow follows a point of the interface between its initial position (at the tail of the arrows) and its position at the end of the film extraction (head of the arrow). These displacements have been measured in the central film, but are only conjectured in the lateral films. The black arrows indicate surfactant diffusion through the bulk and the darker blue domains indicate a simple shear in the liquid phase, due to a velocity difference between both interfaces. (a) Small deformation and/or small velocity: the central film is at rest. (b) Large deformation and large velocity: the central film is compressed. The star indicates a highly stretched domain on the interface.

Based on our observations, we suggest the following scenario for the tangential motions in the film assembly. At small deformation, the central film is not modified by the deformation. The interface velocity field vanishes in the central film, and the top (in red) and bottom (in dark blue) interfaces are respectively stretched and compressed on the lateral films. Adapting the model developed in [12], we expect the external interface (in purple) to flow across the meniscus, from the compressed film to the stretched one, and thus to remain at an interface concentration close to the equilibrium one. As a consequence, in the compressed film, the external interface is at a lower concentration than the bottom one (in blue) and the surfactants should diffuse from the bottom interface to the external one, across the compressed film (black arrow). Once on the external interface, these surfactants are advected toward the stretched interface. They should therefore diffuse again across the stretched film and reach the top interface. This scenario implies some localised shear in the stretched film and in the compressed film, close to the meniscus, as already predicted in [12].

The scenario is similar at higher deformation rate (large displacement and high velocity) but the compression/stretching symmetry is broken. The film extraction observed in the central film is the signature of an interface transfer from the compressed film to the central film, which relaxes the compression in the bottom interface. However, as demonstrated in fig. 4, both interfaces move together in the central film, and the film extraction thus

increases the extension of the top interface, as symbolized by the star in fig. 7. The film extraction thus relaxes the compression of the bottom film and increases the extension of the top interface. This is consistent with the observation made in [12], that the stress generated by the compression exceed the one generated by the stretching.

Conclusion. – In a concentrated suspension of soft solids of typical size L , when one object slides over another one because of an imposed global shear at the rate $\dot{\epsilon}$, the film of continuous phase, of thickness h , trapped between the two objects is sheared at the enhanced rate $\dot{\epsilon}^{loc} \sim \dot{\epsilon}L/h$. This flow cannot be observed when the soft solids are replaced by bubbles, at least for large enough bubbles, because the interfaces cannot support the resulting shear stress. In this letter, using a foaming solution with a large Gibbs modulus, we verify experimentally the absence of shear in a 6 mm large film when a global shear is imposed. The deformation is based, instead, on film compression and extension. At large imposed shear, we observe surfactant transfers from the lateral films to the central film, which is thus surprisingly compressed even if its total area is preserved. This experimental study allows us to propose a possible velocity field in the lateral films, with a localized shear in a small domain close to the meniscus. The direct observation of this conjectured sheared domain is still an experimental challenge, but it should be accessible to the numerical simulation, based on a surfactant transport model.

* * *

This project has received funding from the European Research Council (ERC) under the European Union’s Horizon 2020 research and innovation programme (grant agreement No 725094). We thank M. LE FUR for technical support.

Data availability statement: The data that support the findings of this study are available upon reasonable request from the authors.

REFERENCES

- [1] COHEN-ADDAD S., HÖHLER R. and PITOIS O., *Annu. Rev. Fluid. Mech.*, **45** (2013) 241.
- [2] GOPAL A. D. and DURIAN D. J., *J. Colloid Interface Sci.*, **213** (1999) 169.
- [3] MARZE S., LANGEVIN D. and SAINT-JALMES A., *J. Rheol.*, **52** (2008) 1091.
- [4] DENKOV N. D., TCHOLAKOVA S., GOLEMANOV K., ANANTHAPADMANABHAN K. P. and LIPS A., *Phys. Rev. Lett.*, **100** (2008) 138301.
- [5] LANGLOIS V., HUTZLER S. and WEAIRE D., *Phys. Rev. E*, **78** (2008) 021401.
- [6] GOYON J., COLIN A., OVARLEZ G., AJDARI A. and BOCQUET L., *Nature*, **454** (2008) 84.
- [7] BOCQUET L., COLIN A. and AJDARI A., *Phys. Rev. Lett.*, **103** (2009) 036001.
- [8] BESSON S., DEBRÉGEAS G., COHEN-ADDAD S. and HÖHLER R., *Phys. Rev. Lett.*, **101** (2008) 214504.
- [9] BIANCE A. L., COHEN-ADDAD S. and HÖHLER R., *Soft Matter*, **5** (2009) 4672.
- [10] SATOMI R., GRASSIA P. and OGUEY C., *Colloids Surf. A*, **438** (2013) 77.
- [11] SEIWERT J., MONLOUBOU M., DOLLET B. and CANTAT I., *Phys. Rev. Lett.*, **111** (2013) 094501.
- [12] BUSSONNIÈRE A. and CANTAT I., *J. Fluid Mech.*, **922** (2021) A25.
- [13] CANTAT I., COHEN-ADDAD S., ELIAS F., GRANER F., HÖHLER R., PITOIS O., ROUYER F. and SAINT-JALMES A., *Foams. Structure and Dynamics* (Oxford University Press, Oxford) 2013.
- [14] PRINCEN H. M., *J. Colloid Interface Sci.*, **91** (1983) 160.
- [15] PORYLES R., LENAUVETIER T., SCHAUB E., BUSSONNIÈRE A., SAINT-JALMES A. and CANTAT I., *Soft Matter*, **18** (2022) 2046.
- [16] MYSELS K. J., SHINODA K. and FRANKEL S., *Soap Films: Study of Their Thinning and a Bibliography* (Pergamon, New-York) 1959.
- [17] BRUINSMA R., *Physica A*, **216** (1995) 59.
- [18] GROS A., BUSSONNIÈRE A., NATH S. and CANTAT I., *Phys. Rev. Fluids*, **6** (2021) 024004.
- [19] SHABALINA E., BÉRUT A., CAVELIER M., SAINT-JALMES A. and CANTAT I., *Phys. Rev. Fluids*, **4** (2019) 124001.